APL Materials ARTICLE scitation.org/journal/apm

The other model antiferroelectric: $PbHfO_3$ thin films from ALD precursors

Cite as: APL Mater. 9, 021108 (2021); doi: 10.1063/5.0035730
Submitted: 30 October 2020 • Accepted: 2 January 2021 •
Published Online: 4 February 2021

View Online

Export Citation

CrossMark

Brendan Hanrahan,[1,a)] Cosme Milesi-Brault,[2,3] Asher Leff,[1,4] Alexis Payne,[1,5] Shi Liu,[6,7] Mael Guennou,[3,8] and Nicholas Strnad[1]

AFFILIATIONS

[1] Sensors and Electron Devices Directorate, U.S. Army Research Laboratory, Adelphi, Maryland 20783, USA
[2] Materials Research and Technology Department, Luxembourg Institute of Science and Technology, 41 rue du Brill, L-4422 Belvaux, Luxembourg
[3] Inter-Institutional Research Group Uni.lu-LIST on Ferroic Materials, 41 rue du Brill, L-4422 Belvaux, Luxembourg
[4] General Technical Services, LLC, Wall, New Jersey 07727, USA
[5] Materials Science and Engineering Department, North Carolina State University, Raleigh, North Carolina 27606, USA
[6] School of Science, Westlake University, Hangzhou, Zhejiang 310024, China
[7] Institute of Natural Sciences, Westlake Institute for Advanced Study, Hangzhou, Zhejiang 310024, China
[8] Department of Physics and Materials Science, University of Luxembourg, 41 rue du Brill, L-4422 Belvaux, Luxembourg

Note: This paper is part of the Special Topic on 100 Years of Ferroelectricity—A Celebration.
[a)] **Author to whom correspondence should be addressed:** brendan.m.hanrahan.civ@mail.mil

ABSTRACT

Antiferroelectric $PbHfO_3$ is grown from atomic layer deposition precursors lead bis(dimethylaminomethylpropanolate) and tetrakis dimethylamino hafnium with H_2O and O_3 oxidizers in thicknesses from 20 nm to 200 nm at a substrate temperature of 250 °C. X-ray analysis shows an as-grown crystalline PbO phase that diffuses into an amorphous HfO_2 matrix upon annealing to form a randomly oriented, orthorhombic $PbHfO_3$ thin film. Electrical characterization reveals characteristic double hysteresis loops with maximum polarizations of around 30 $\mu C/cm^2$ and transition fields of 350 kV/cm–500 kV/cm depending on the thickness. Temperature-dependent permittivity and polarization testing show a phase transition at 185 °C, most probably to the paraelectric phase, but give no clear evidence for the intermediate phase known from bulk $PbHfO_3$. The energy storage density for the films reaches 16 J/cm^3 at 2 MV/cm. A dielectric tunability of 221% is available within 1 V for the thinnest film. These results highlight the unique spectrum of properties available for thin film perovskite antiferroelectrics.

© 2021 Author(s). All article content, except where otherwise noted, is licensed under a Creative Commons Attribution (CC BY) license (http://creativecommons.org/licenses/by/4.0/). https://doi.org/10.1063/5.0035730

I. INTRODUCTION

Antiferroelectrics (AFE) are recognized experimentally by a phase transition between two non-polar phases accompanied by a dielectric anomaly and a characteristic double polarization hysteresis loop arising from an electric field-induced phase transition from a non-polar to a polar phase. The properties of this transition make AFEs excellent for energy storage,[1] power conditioning,[2] and upcoming electronic memory applications.[3] The archetype AFE perovskite is considered to be $PbZrO_3$ (PZO), identified as early as 1951.[4] Here, we investigate the closely related perovskite $PbHfO_3$ (PHO). It was recognized in 1953 that the crystal structure of PHO was similar to the archetypical AFE PZO, although only a linear dielectric behavior was observed at that time.[5] Subsequent studies on bulk PHO confirmed the structure,[6] but the evidence for a truly antiferroelectric behavior, i.e., the field-induced phase transition and its characteristic double loop, was only reported in 1980. Besides, PHO differs from PZO by the presence of an intermediate phase consistently observed between the paraelectric cubic phase and the orthorhombic antiferroelectric *Pbam* phase.[5] This intermediate phase is observed between 160 °C and 215 °C and is often referred to as AFE_1, although there is very little evidence that

this phase is really antiferroelectric itself. It was recently identified as incommensurate.[7] Generally speaking, PHO has been much less investigated than PZO, bulk or thin film. In particular, to the best of our knowledge, there is no reported electrical characterization on thin film PHO aside from the hysteresis loop in our recent work on PHO film growth.[8]

The AFE-FE phase transition has been noted as an energy storage mechanism since the 1960s,[9] and therefore, these materials are considered for applications such as pulsed power, lasers, radar, and power inverters, which require high energy storage density (ESD) electrostatic capacitors.[10]

In the bulk, PHO prepared by rolling and conventional sintering was clearly AFE, with an energy storage density of 7.6 J/cm^3 for a bulk material.[11] Recent advances in ultra-thin, atomic-layer deposited AFE-like materials have shown high ESDs, namely, Si-doped,[12] Al-doped,[13] and Zr-rich[14] compositions and combinations thereof[15] of ferroelectric hafnia. Owing to thin, conformal coating, new regimes of ESD have been reached.[16] However, the characteristic properties of Pb-based ferroelectrics such as high polarization, low coercive field, and high permittivity are not available within the hafnium oxide material system.

II. DEVICE FABRICATION

Metal–insulator–metal (MIM) capacitors were fabricated in order to investigate the electrical properties of the PHO films grown by atomic layer deposition (ALD). The 100 nm-thick platinum bottom electrode was formed on a $TiO_2/SiO_2/Si$ substrate stack.[17] The ALD PHO films were grown using a super-cycle of HfO_2 and PbO_x constituent binary oxide processes in a *Kurt Lesker ALD 150-LX* platform. The binary PbO_x process was performed using 98%-purity lead bis(dimethylaminomethylpropanolate) [$Pb(DMAMP)_2$] procured from *Strem Chemicals Inc.* The $Pb(DMAMP)_2$ was held at 90 °C and was oxidized using a combination of H_2O and ozone. The cation composition was varied by changing the relative number of PbO_x:HfO_2 cycles. Details of the growth can be found in a previous publication by Strnad *et al.*[8] PHO near the ideal $PbHfO_3$ stoichiometry was achieved using a 3:1 PbO_x:HfO_2 cycle-ratio at a substrate temperature of 250 °C. The growth kinetics of the ALD PHO were measured *in situ* using an ellipsometer, which indicated a linear growth rate of 0.07 nm/cycle. The specific cation precursors, oxidizer combinations, and dose/purge times were nearly identical to that reported for ALD $PbTiO_3$ in a separate work by Strnad *et al.*,[18] except that tetrakis dimethylamino hafnium (TDMAH) was substituted for tetrakis dimethylamino titanium. Three thicknesses were grown: 20 nm, 50 nm, and 200 nm. After film growth, Pt was sputtered at room temperature and electrodes were defined using a lift-off process. Samples were then annealed at 700 °C or 800 °C for 1960s in an oxygen environment. Sample composition was measured after heat treatments using Rutherford backscattering analysis showing stoichiometric PHO within the error.

III. MATERIAL CHARACTERIZATION

Structural characterization was performed with grazing-incidence X-ray diffraction (GIXRD) and transmission electron microscopy (TEM). Diffractograms of the as-deposited material in Fig. 1(a) show the presence of crystalline peaks coinciding with the litharge phase of lead oxide (PDF Card: 00-005-0570). This supports the observations from Strnad *et al.* that the Pb precursor does not wet the surface but instead forms a segregated, crystalline phase.[8] With increasing thickness, we observe the emergence of thinner Bragg peaks and a general increase in intensity that we attribute to a combination of size effect, improvement in crystallinity, and increase in volume. The annealed film diffractograms [Fig. 1(b)] show a randomly oriented PHO film (PDF card: 04-012-0549) with no significant differences in preferred orientation among the film thicknesses. If the crystallization proceeded from the bottom electrode, as it does with many deposition techniques, then the orientation would be expected to change as the film thickness is increased and stress can be relieved.[19] These results support earlier observations[8] and suggest that PHO from ALD precursors crystallizes by interdiffusion of an amorphous HfO_2 matrix with isolated crystalline PbO regions. The interdiffusion-driven growth process will make it difficult to use conventional techniques for thin film stress tuning and templating. The film stress and the ability to template growth from oriented electrodes or seeds may be affected by this unique growth process.

Transmission electron microscopy (TEM) characterization was carried out using a probe-corrected JEOL ARM 200F operated at 200 keV in both conventional and scanning modes. The specimen was prepared using a *Thermofisher Helios* 4 focused ion beam/scanning electron microscope. TEM characterization showed that the ~50 nm PHO had a columnar microstructure with grains going all the way through the thickness of the film. The film thickness ranged from 54 nm to 60 nm due to roughness in both the bottom Pt electrode and the film itself. Scanning TEM-high angular annular dark field (STEM-HAADF) images, which provide mass-thickness contrast, show small, spherical pores in the interior of the film, particularly along grain boundaries, with larger, hemispherical pores along the surface of the film adjacent to the interface with the top Pt electrode (Fig. S1). One possibility is that these pores represent volumes previously occupied by crystalline PbO, which was integrated during annealing or evaporated, as it is has been observed in lead zirconate titanate (PZT).[20] Further work is needed to optimize the thermal processing to reduce the porosity. While both Pt layers exhibit a columnar microstructure, the top electrode also exhibited intergranular pores possibly from the room-temperature sputtering process, whereas the bottom did not. Fast Fourier transforms of high resolution TEM (HRTEM) images of the PHO layer were indexed to confirm that the PHO has an orthorhombic crystal structure (space group 55—*Pbam*) with lattice parameters a = 0.5856 nm, b = 1.1729 nm, and c = 0.8212 nm, which is in agreement with previous studies on bulk crystals.[21]

Figure 2(a) shows the dielectric hysteresis loops at 1 kHz for the 20 nm, 50 nm, and 200 nm films obtained using the *Radiant Precision Premier II* testing system. The electrode areas were either 1.81 or 0.492×10^{-3} cm^2. Each thickness shows a classical AFE character with AFE → FE fields decreasing with increasing thickness. The trend observed in this study aligns with previous works where thinner films have a lower polarization and an increase in E_f,[22] but the precise origin is unknown. Stress is a factor affecting the phase transition field.[23] The XRD study in Figs. 1(a) and 1(b) suggests that there are no large residual stress differences among the thicknesses but thermal stress due to the thermal expansion mismatch between the film and substrate are thickness-dependent.[24] Another

© Author(s) 2021

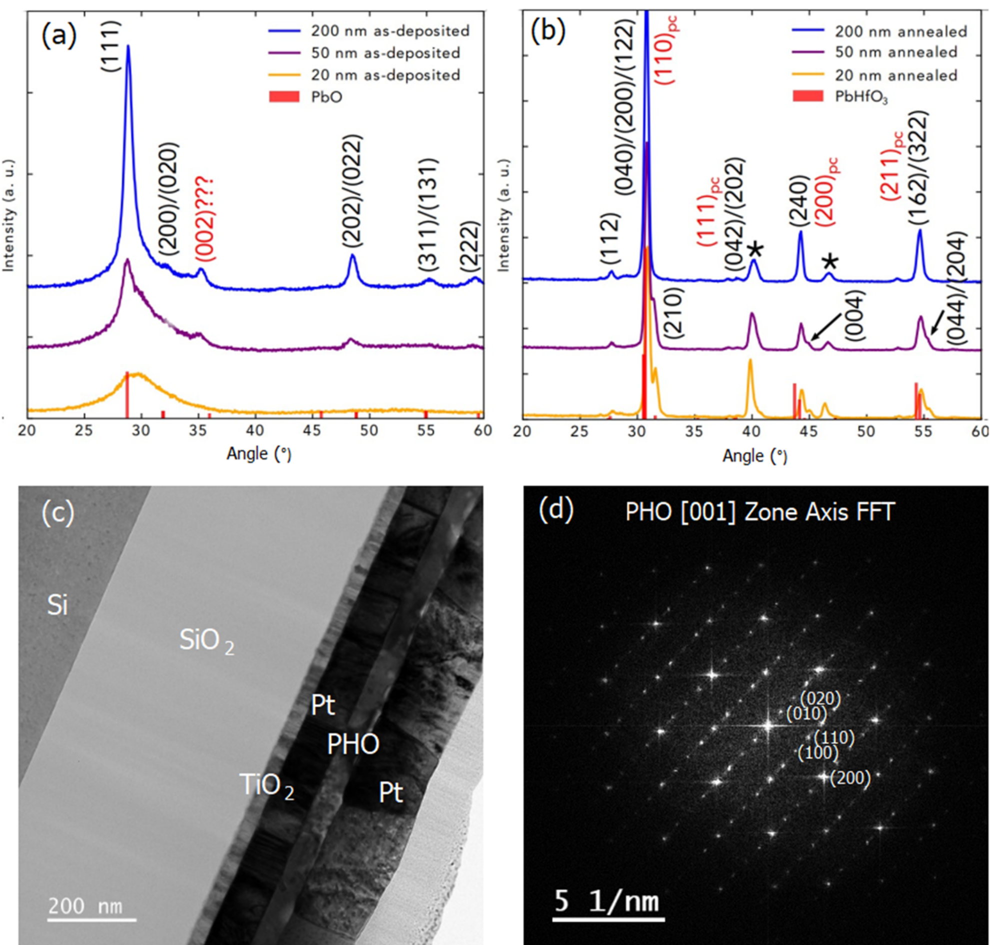

FIG. 1. GIXRD of (a) as-deposited and (b) post annealed PHO thin films. For PHO, stars indicate the Pt substrate peaks and red labels with the pc subscript indicate the equivalent peak in the pseudo-cubic notation. (c) Cross section TEM image of the film stack and (d) indexed fast Fourier transform (FFT) from a [001] zone axis-oriented PHO grain.

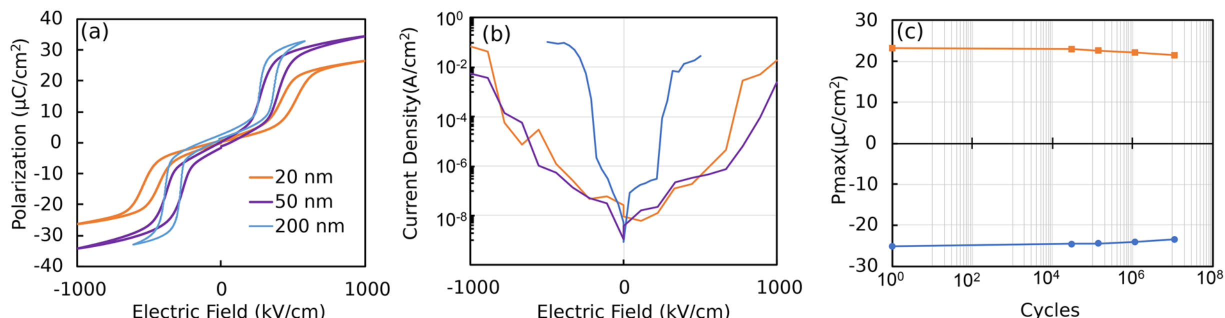

FIG. 2. (a) Polarization hysteresis loops for 20 nm, 50 nm, and 200 nm $PbHfO_3$ films taken at 1 kHz. (b) Current – voltage relationships for each thickness measured by averaging 100 ms after a 1 s hold at each voltage step, and (c) fatigue measurements showing maximum polarization for the 20 nm film taken at 10 kHz, 1.5 V(750 kV/cm), square wave stimulation.

© Author(s) 2021

explanation is that the AFE material has a "dead layer" analogous to the dead layers for ferroelectric films,[25] i.e., a low-permittivity, fully linear dielectric region in series with the AFE one so that an increase in E_f and a reduction in P_{max} would be expected with decreasing sample thickness.[25] The cross-sectional TEM inspection did not reveal the presence of an interfacial layer but the samples trend in accordance with this explanation. Finally, domain mobility is known to contribute to scaling effects on the coercive fields of ferroelectrics, where $E_c \propto d^{-2/3}$,[26] but this scaling becomes less accurate once grains are small enough to only contain a single domain, around 100 nm.[27]

For all of the samples, the coercive field is <25% of hafnia ferroelectrics.[28] The lower coercive field can reduce power requirements for devices like AFE field effect transistors (AFEFeT) that take advantage of the non-polar gate dielectric to reduce gate-induced drain leakage.[29] Unexpectedly, the 200 nm film had the highest leakage current density and lowest breakdown voltage [Fig. 2(b)]. The porosity observed in the 50 nm sample in TEM is expected in the 200 nm sample, which acts as a field concentration center.[30] The local concentrations of the electric field increase leakage current and provide nucleation sites for breakdown.

Compared to AFE-like hafnia materials, the AFE phase of PHO is the thermodynamically stable zero field state that may provide long-term stability advantages. In Fig. 2(c), the maximum polarization is shown up to 10^7 cycles for the 20 nm PHO sample after the AFE has been stimulated by a square wave at 1.5 V and 10 kHz. AFE-like $Al:HfO_2$ change to the FE phase after 10^5 cycles,[31] while $Si:(Hf,Zr)O_2$ maintains the AFE-like phase past 10^9 cycles,[15] which is in agreement with observations of related antiferroelectrics.[32]

In order to get more insight into the material properties and the stability of the antiferroelectric switching behavior, the dielectric properties were investigated as a function of temperature up to 300 °C for the 50 nm PHO sample (Fig. 3). Figure 3(a) shows polarization as a function of field and temperature, where clear double hysteresis loops are observed up to elevated temperatures. The dielectric constant and loss tangent tan(δ) measured using a *TF Analyzer* 2000 from *aixACCT* at a frequency of 5 kHz with an oscillating voltage of 100 mV as a function of temperature are reported in Fig. 3(b).

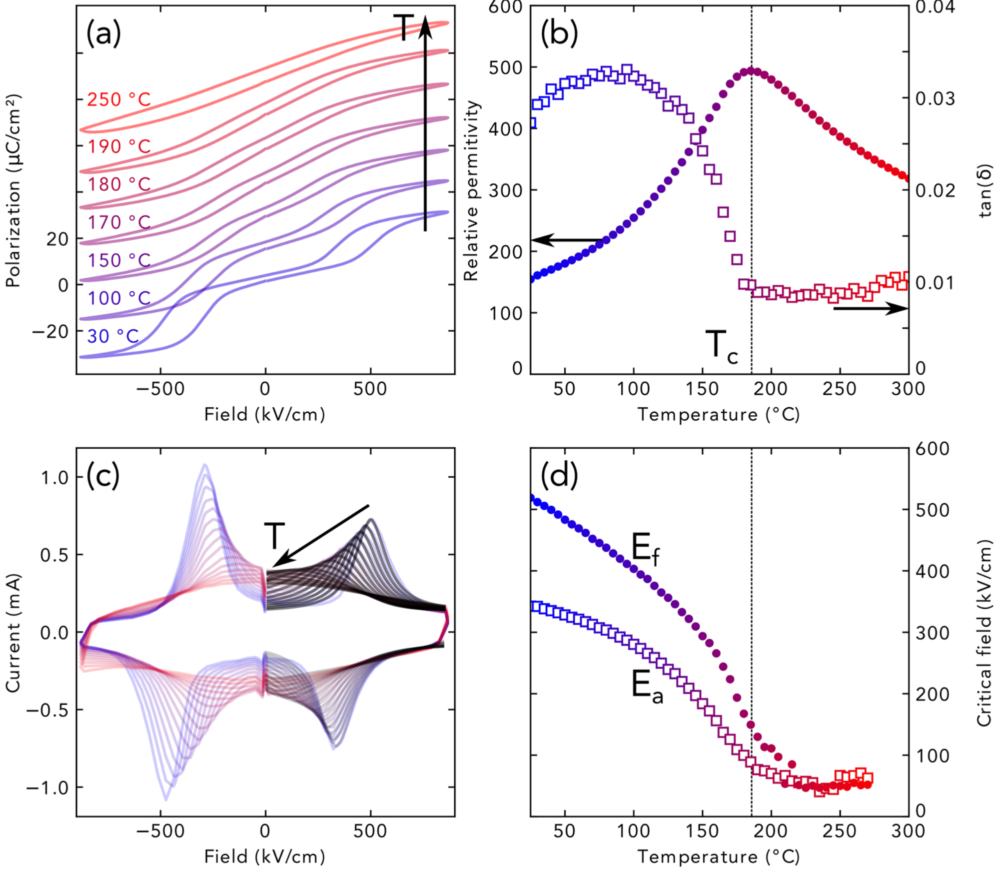

FIG. 3. (a) Polarization curves P(E) at different temperatures and (b) temperature-dependency of the relative permittivity of a 50 nm-thick PHO film. The dielectric anomaly shows a single transition at 185 °C. (c) Current curves I(E) of the same sample at different temperatures. Black lines show the asymmetrical pseudo-Voigt fits performed to follow the position in field of the extrema of current in the positive field part. These extracted critical fields are reported on (d).

© Author(s) 2021

We observe a steady increase in the dielectric constant that reaches a peak around T = 185 °C before decreasing again, which matches the shape expected for an AFE transition. In addition, In order to determine an E–T phase diagram, we tentatively determined the critical electric fields as a function of T by taking the maximum of current (I) curves vs field. This was done by fitting the I(E) data with an asymmetric peak (of no particular physical significance), as illustrated in Fig. 3(c). Both the switching field E_f and the backswitching field E_a decrease gradually with increasing temperature. However, they [Fig. 3(d)] do not drop to zero at T_c, as it could have been expected from past examples of E–T phase diagrams[33] or phenomenological theory.[34] Instead, both values of E_f and E_a seem to reach a plateau above 200 °C, suggesting that these extracted fields above T_c might not have a physical meaning. Indeed, if the material had stabilized in a ferroelectric or antiferroelectric phase, this critical field should vary with temperature. Further work is needed to clarify the interpretation for this and check whether this field corresponds to a structural transition or not. Also remarkable is the fact that the dielectric data do not show any clear evidence for the intermediate phase known in bulk PHO. The maximum of permittivity falls in between the temperatures of the two transitions observed in bulk PHO around 160 °C and 210 °C.[35,36] It is possible that the difference between the two phases is not captured by these dielectric measurements, but it could also be that the intermediate phase is suppressed in thin films due to strain or other effects. Further structural studies will be needed to clarify this issue; first principle calculations could also help to evaluate the robustness of this intermediate phase against the strain expected in thin films.

IV. ELECTRICAL PERFORMANCE

We now discuss these properties in the perspective of various electrical applications. Figure 4(a) shows the ESD and storage efficiency for each film thickness. ESD increases dramatically at the AFE-FE transition field, reaching ~8 J/cm^3 at 450 kV/cm and doubling at dielectric breakdown at 2000 kV/cm. The storage efficiency is observed by the slimness of the hysteresis loop, or the difference in $E_f - E_a$, which has been shown to be reducible by doping lead lanthanum zirconated titanate (PLZT).[37] The state of the art for hafnia-based AFE-like materials is closer to 60 J/cm^3 and 80% efficiency at electric fields of 4500 kV/cm.[28] Although the ESD is much

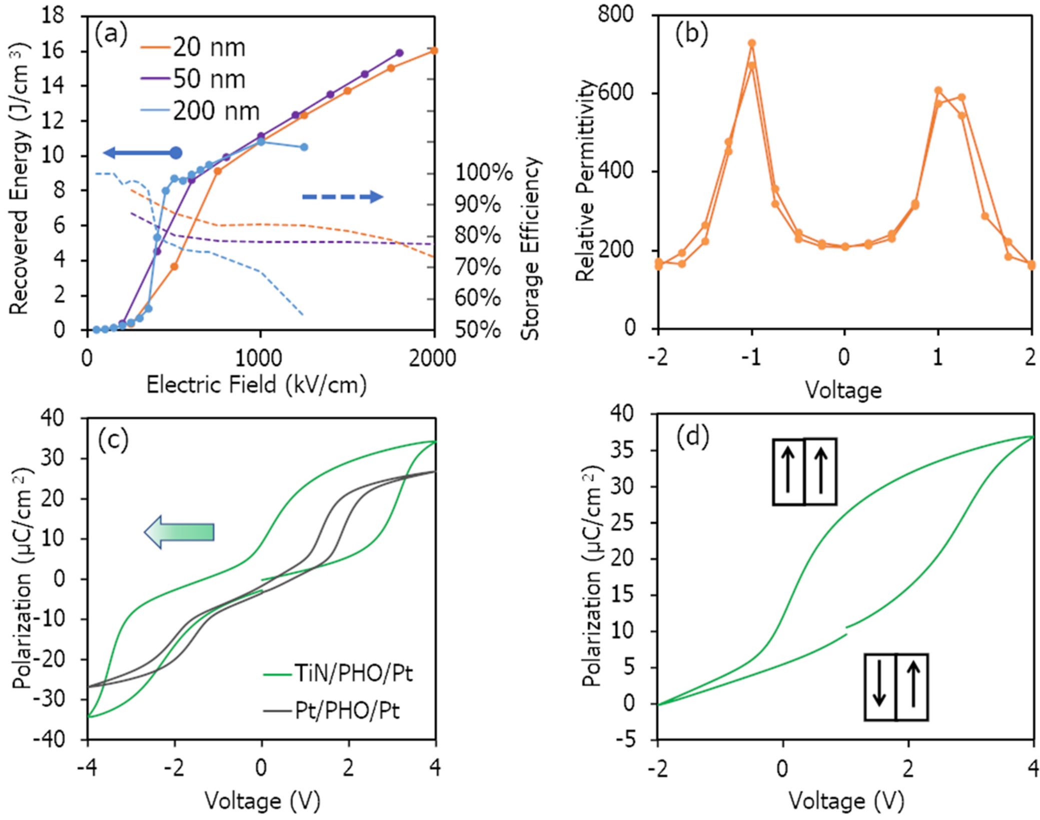

FIG. 4. (a) Energy storage density for each film thickness calculated from monopolar hysteresis data taken at 10 kHz. (b) Permittivity for the 20 nm film. (c) Polarization hysteresis measured for PHO capacitors with either TiN or Pt top electrodes with arrow indicating direction of imprint and (d) minor loop of the TiN sample centered at 1 V where the polarization states are graphically depicted.

© Author(s) 2021

higher, the lower electric field values merit examinations. Compared to the PHO ESD, it requires >2000 kV/cm vs 450 kV/cm for AFE-like HFO to reach the ~8 J/cm^3 storage density. While ESD is a useful figure for comparison, the driver of pulsed power applications is the energy, which will depend on the product of film geometry and ESD. Having higher energy storage densities at lower fields could be a benefit since the voltage will increase as the film thickness increases.

Capacitance density is an important metric for compact power conditioning applications. In Fig. 4(b), we show the relative permittivity of the 20 nm PHO sample measured using an *HP* 4192*A* network analyzer with an oscillating voltage and frequency of 50 mV and 10 kHz, respectively. The permittivity varies from ε = 200–600 at the phase transition and then <200 in the region of ferroelectric saturation. There are two implications derived from the permittivity data: first, the capacitance density of these films will be around ten times higher than hafnia films of an equivalent thickness and a permittivity of 20, and second, the films show a tunability of 221% within 1 V calculated from

$$\text{Tunability}(\%) = [\varepsilon(E_o) - \varepsilon(E)]/\varepsilon(E_o) \times 100\%. \quad (1)$$

PHO could have applications in low power microwave applications, where recently, simulations of hafnia ferroelectrics have shown promise taking advantage of the tunability over a small applied voltage range.[38]

FE random access memory (FRAM), which relies on nonvolatile positive and negative polarization states, has recently been reimagined by Pesic *et al.* for AFEs where the two states are poled and un-poled.[39] Both states are made accessible at 0 V by significantly imprinting the hysteresis loop such that the AFE+ → FE+ transition is at positive biases and the FE+→AFE + transition is at negative biases. This work is motivated by the generally superior fatigue performance of AFEs vs FEs. Figure 4(c) shows the polarization hysteresis for a symmetrical 20 nm Pt/PHO/Pt capacitor and the same material with an asymmetrical electrode configuration of TiN/PHO/Pt. A minor loop of +/−3 V taken with a DC bias of 1 V appears nearly identical to a ferroelectric polarization [Fig. 4(d)] but with non-polar and polar states.

In addition to potential imprint, the maximum polarization and field width of the AFE → FE hysteresis widened with the addition of a TiN electrode. It is challenging to de-convolute asymmetrical changes in polarization and coercive fields within the polarization hysteresis because the measurement is self-centering, and therefore, vertical shifts of unsaturated loops can appear as imprint. An assumption that the TiN generated an oxygen-depleted TiO_xN_y interface would increase E_f but not clearly increase polarization. PZO films of similar thicknesses grown epitaxially with pulsed-laser deposition show polarization values ~45 μC/cm^2[40] compared to PHO showing ~30 μC/cm^2, so the increase in P_{max} associated with the TiN could be associated with a de-pinning of domains at the electrode interface. The leakage current reduced for the TiN device but gained a strong bias-dependent asymmetry, while the fatigue suffered, failing after 10^5 cycles. Further work is needed to fully realize PHO films imprinted, centered on 0 V.

V. SUMMARY AND CONCLUSION

In summary, antiferroelectric $PbHfO_3$ films show a unique combination of properties, namely, transition fields, permittivity, and polarization compared to the similarly thick hafnia-based films. The structural and electrical analysis reveals both similarities and differences to the isomorphic PZO with an added benefit of more reliable ternary ALD growth from hafnia precursors vs zirconia.[8] The unique crystallization route for PHO from ALD precursors may be exploited to lower the crystallization temperature. Further work should focus on process optimization to establish a minimum crystallization temperature, reduce porosity, and manipulate stress to tailor the E_f field for specific applications. The pyroelectric and electrocaloric performance of Pb-based AFEs is excellent,[41,42] so further investigation in PHO is warranted. The potential for electronic device integration, particularly through imprinting the AFE, also merits further investigation. Finally, the electric field–temperature phase diagram suggested by our study disagrees with previous observations on PHO ceramics where an intermediate phase is observed in the temperature dependence of permittivity and with x-ray diffraction, so film stress implications need to be better understood. PHO is a classic antiferroelectric identified over 60 years ago, which could realize new physics and applications as a thin film.

SUPPLEMENTARY MATERIAL

See the supplementary material for scanning transmission electron microscopy high-angle annular dark-field imaging of the thin film $PbHfO_3$.

ACKNOWLEDGMENTS

The authors would like to acknowledge the Army Research Laboratory (ARL) Specialty Electronic Materials and Sensors Cleanroom (SEMASC) Nanofabrication Facility for their assistance with device fabrication. C.M.-B. and M.G. acknowledge financial support by the Luxembourg National Research Fund under Project No. BIAFET C16/MS/11348912/Guennou.

DATA AVAILABILITY

The data that support the findings of this study are available from the corresponding author upon reasonable request.

REFERENCES

[1] Z. Liu, T. Lu, J. Ye, G. Wang, X. Dong, R. Withers, and Y. Liu, Adv. Mater. Technol. **3**, 1800111 (2018).
[2] S. Kwon, W. Hackenberger, E. Alberta, E. Furman, and M. Lanagan, IEEE Electr. Insul. Mag. **27**, 43 (2011).
[3] M. Pešić, M. Hoffmann, C. Richter, T. Mikolajick, and U. Schroeder, Adv. Funct. Mater. **26**, 7486 (2016).
[4] G. Shirane, E. Sawaguchi, and Y. Takagi, J. Phys. Soc. Jpn. **6**, 208 (1951).
[5] G. Shirane and R. Pepinsky, Phys. Rev. **91**, 812 (1953).
[6] O. E. Fesenko and L. E. Balyunis, Ferroelectrics **29**, 95 (1980).

© Author(s) 2021

[7] A. Bosak, V. Svitlyk, A. Arakcheeva, R. Burkovsky, V. Diadkin, K. Roleder, and D. Chernyshov, Acta Crystallogr., Sect. B: Struct. Sci., Cryst. Eng. Mater. **76**, 7 (2020).
[8] N. A. Strnad, B. Hanrahan, D. M. Potrepka, J. S. Pulskamp, R. J. Phaneuf, and R. G. Polcawich, J. Am. Ceram. Soc. **104**(3), 1216–1228 (2020).
[9] B. Jaffe, Proc. IRE **49**, 1264 (1961).
[10] C. W. Ahn, G. Amarsanaa, S. S. Won, S. A. Chae, D. S. Lee, and I. W. Kim, ACS Appl. Mater. Interfaces **7**, 26381 (2015).
[11] J. Wei, T. Yang, and H. Wang, J. Eur. Ceram. Soc. **39**, 624 (2019).
[12] F. Ali, X. Liu, D. Zhou, X. Yang, J. Xu, T. Schenk, J. Müller, U. Schroeder, F. Cao, and X. Dong, J. Appl. Phys. **122**, 144105 (2017).
[13] W. L. Zhang, Y. H. Mao, L. Cui, M. H. Tang, P. Y. Su, X. J. Long, Y. G. Xiao, and S. A. Yan, Phys. Chem. Chem. Phys. **22**, 21893 (2020).
[14] M. H. Park, H. J. Kim, Y. J. Kim, T. Moon, K. D. Kim, and C. S. Hwang, Adv. Energy Mater. **4**, 1400610 (2014).
[15] P. D. Lomenzo, C.-C. Chung, C. Zhou, J. L. Jones, and T. Nishida, Appl. Phys. Lett. **110**, 232904 (2017).
[16] K. Kühnel, M. Czernohorsky, C. Mart, and W. Weinreich, J. Vac. Sci. Technol., B **37**, 021401 (2019).
[17] G. R. Fox, D. M. Potrepka, and R. G. Polcawich, J. Mater. Sci.: Mater. Electron. **29**, 412 (2018).
[18] N. A. Strnad, D. M. Potrepka, J. S. Pulskamp, Y. Liu, J. L. Jones, R. J. Phaneuf, and R. G. Polcawich, J. Vac. Sci. Technol., A **37**, 020917 (2019).
[19] J. P. de la Cruz, E. Joanni, P. M. Vilarinho, and A. L. Kholkin, J. Appl. Phys. **108**, 114106 (2010).
[20] N. Izyumskaya, Y.-I. Alivov, S.-J. Cho, H. Morkoç, H. Lee, and Y.-S. Kang, Crit. Rev. Solid State Mater. Sci. **32**, 111 (2007).
[21] D. L. Corker, A. M. Glazer, W. Kaminsky, R. W. Whatmore, J. Dec, and K. Roleder, Acta Crystallogr., Sect. B: Struct. Sci. **54**, 18 (1998).
[22] B. Xu, Y. Ye, Q.-M. Wang, and L. E. Cross, J. Appl. Phys. **85**, 3753 (1999).
[23] J. Ge, D. Remiens, X. Dong, Y. Chen, J. Costecalde, F. Gao, F. Cao, and G. Wang, Appl. Phys. Lett. **105**, 112908 (2014).
[24] J.-L. Cao, A. Solbach, U. Klemradt, T. Weirich, J. Mayer, U. Böttger, U. Ellerkmann, P. J. Schorn, P. Gerber, and R. Waser, J. Am. Ceram. Soc. **89**, 1321 (2006).
[25] Y. Sakashita, H. Segawa, K. Tominaga, and M. Okada, J. Appl. Phys. **73**, 7857 (1993).
[26] P. Chandra, M. Dawber, P. B. Littlewood, and J. F. Scott, Ferroelectrics **313**, 7 (2004).
[27] S. B. Ren, C. J. Lu, J. S. Liu, H. M. Shen, and Y. N. Wang, Phys. Rev. B **54**, R14337 (1996).
[28] M. H. Park and C. S. Hwang, Rep. Prog. Phys. **82**, 124502 (2019).
[29] J. Kavalieros, I. Young, M. Metz, U. Avci, C.-C. Lin, O. Loh, S. H. Sung, A. Kasukurti, S.-C. Chang, T. Gosavi, and A. V. Penumatcha, in USPTO Report Uspto (Intel Corporation, USA, 2020); available at https://patents.google.com/patent/US20200312978A1/en.
[30] Y. Podgorny, K. Vorotilov, P. Lavrov, and A. Sigov, Ferroelectrics **503**, 77 (2016).
[31] K. Florent, S. Lavizzari, M. Popovici, L. Di Piazza, U. Celano, G. Groeseneken, and J. Van Houdt, J. Appl. Phys. **121**, 204103 (2017).
[32] J. H. Jang, K. H. Yoon, and K. Y. Oh, Mater. Res. Bull. **35**, 393 (2000).
[33] S. Horiuchi, R. Kumai, and S. Ishibashi, Chem. Sci. **9**, 425 (2018).
[34] P. Tolédano and M. Guennou, Phys. Rev. B **94**, 014107 (2016).
[35] G. A. Samara, Phys. Rev. B **1**, 3777 (1970).
[36] J.-H. Ko, K. Roleder, A. Majchrowski, and A. Bussmann-Holder, J. Korean Phys. Soc. **64**, 1169 (2014).
[37] N. K. Gözüaçık, E. Mensur-Alkoy, and S. Alkoy, J. Mater. Sci.: Mater. Electron. **30**, 14045 (2019).
[38] M. Dragoman, M. Aldrigo, M. Modreanu, and D. Dragoman, Appl. Phys. Lett. **110**, 103104 (2017).
[39] M. Pesic, L. Larcher, T. Mikolajick, T. Li, V. Di Lecce, M. Hoffmann, M. Materano, C. Richter, B. Max, S. Slesazeck, and U. Schroeder, IEEE J. Electron Devices Soc. **6**, 1019 (2018).
[40] R. Gao, S. E. Reyes-Lillo, R. Xu, A. Dasgupta, Y. Dong, L. R. Dedon, J. Kim, S. Saremi, Z. Chen, C. R. Serrao, H. Zhou, J. B. Neaton, and L. W. Martin, Chem. Mater. **29**, 6544 (2017).
[41] B. Hanrahan, Y. Espinal, S. Liu, Z. Zhang, A. Khaligh, A. Smith, and S. P. Alpay, J. Mater. Chem. C **6**, 9828 (2018).
[42] R. Pirc, B. Rožič, J. Koruza, B. Malič, and Z. Kutnjak, Europhys. Lett. **107**, 17002 (2014).

© Author(s) 2021